Valence mirror symmetry between $Z = 50$ isotopes and $N = 82$ isotones

Y. Y. Zong [1], C. Ma [1], H. Jiang [2] and Y. M. Zhao [1,3,*]

[1] *Shanghai Key Laboratory of Particle Physics and Cosmology, School of Physics and Astronomy, Shanghai Jiao Tong University, Shanghai 200240, China*

[2] *School of Science, Shanghai Maritime University, Shanghai 201306, China*

[3] *Collaborative Innovation Center of IFSA (CICIFSA), Shanghai Jiao Tong University, Shanghai 200240, China*

(Received 14 July 2023; revised 1 September 2023; accepted 16 May 2024; published 7 June 2024)

In this paper we study the valence mirror symmetry between the Sn ($Z = 50$) isotopes and $N = 82$ isotones, in the frameworks of the nuclear shell model (NSM) and its nucleon-pair approximation (NPA). The NPA energy spectra and electromagnetic properties for yrast states are well consistent with the shell-model results as well as available data in experiments. Remarkable correspondences of the energy spectra and electromagnetic matrix elements between the even-even Sn isotopes and $N = 82$ isotones are emphasized in both the experimental data and theoretical calculations. The asymmetry of $E_{2_1^+}$ values are explained in terms of the evolution of single-particle energy splitting between the $1g_{7/2}$ and $2d_{5/2}$ orbits for the $N = 82$ isotones.

DOI: 10.1103/PhysRevC.109.064306

I. INTRODUCTION

Isospin symmetry is a fundamental concept in nuclear physics. With this symmetry, the nuclear force is charge independent and thus exhibits identical behavior for neutrons and protons [1]. This leads to the fact that energy spectra and electrodynamic properties of one-pair mirror nuclei, one with Z protons and N neutrons and the other with N protons and Z neutrons, display remarkable similarities. Similar to the symmetry of mirror nuclei, Refs. [2–6] suggested another regular pattern, the so-called valence mirror symmetry in one pair of nuclei, with valence particles in the same valence space but outside different magic cores. This symmetry is especially pronounced in nuclei pairs that are singly magic, and the best examples are the Sn ($Z = 50$) isotopes and $N = 82$ isotones, because they have very long chains, thus providing us with the unique opportunity to study the valence mirror symmetry. However, previous studies of valence mirror symmetry for the Sn isotopes and corresponding $N = 82$ isotones focused on cases with relatively larger valence nucleons (pair number larger than 5), partly due to the unavailability of experimental data for relevant nuclei 20 years ago.

In last two decades, the Sn isotopes have been of both experimental [7–16] and theoretical [17–26] interest; the low-lying states of $N = 82$ isotones were studied theoretically in terms of the nucleon-pair approximation (NPA), the nuclear shell model (NSM), and the relativistic quasiparticle random phase approximation (QRPA) [27–33], and the seniority structure of the $N = 82$ isotones is of particular interest in shell-model calculations [34–39]. However, few studies discussed the valence mirror symmetry between them, if any.

Therefore it is both timely and interesting to revisit the low-lying structure of the Sn isotopes and $N = 82$ isotones on the same footing, and, meanwhile, to investigate the valence mirror symmetry between these two chains. This paper is organized as follows. In Sec. II, we explain briefly the framework of the NPA, including the parametrizations of the Hamiltonian and the nucleon-pair basis. In Sec. III, we present our NSM and NPA calculations for the low-lying states of both even-even and odd-mass Sn isotopes and for those of corresponding $N = 82$ isotones. The symmetry and asymmetry in these valence mirror nuclei are discussed extensively. In Sec. IV, we give the summary and conclusion of this paper.

II. THEORETICAL FRAMEWORK

The NPA is a powerful tool of truncating the gigantic shell model configuration space. There have been a number of widely used NPA forms, such as the generalized seniority scheme [40], the broken pair approximation [41], and the fermion dynamical symmetry model [42,43]. The NPA has also been used to study the microscopic foundations of the interacting-boson model (IBM) [44]. In 1997, a generalized NPA formalism was proposed by Chen [45]; since then a number of versions of the NPA were suggested, and here we mention a few [46–51]. A comprehensive review of the NPA can be found in Ref. [52].

In the NPA calculations, the collective nucleon pairs with angular momentum r and projection M are defined as

$$A_M^{r\dagger} = \sum_{jj'} y(jj'r)(C_j^\dagger \times C_{j'}^\dagger)_M^{(r)\dagger}. \tag{1}$$

Here $C_j^\dagger$ is the creation operator of single-j orbit and r denotes the angular momentum of the nucleon pair. $y(jj'r)$ are usually called structure coefficients. The nucleon-pair basis is

*Corresponding author: ymzhao@sjtu.edu.cn

constructed by successively operating $A^{r\dagger}$ on the vacuum state in the valence space. If one considers all possible nucleon pairs, the NPA is equivalent to the NSM. In most cases, only one-type nucleon pairs for one given spin are adopted to minimize the configuration space, as in the IBM.

In this work, we use collective S, D, G, G', I, and F pairs, with spins and parities $r = 0^+$, 2^+, 4^+, 4^+, 6^+, and 3^-. Their structure coefficients are obtained as follows. For S pairs, we diagonalize the Hamiltonian H in the $(S_j^\dagger)^N|0\rangle$ space, while j runs over all the single-particle levels. By using the χ^2-fitting procedure, we obtain the structure coefficients with the $(S^\dagger)^N|0\rangle$ state reaching the maximum overlap with the lowest-energy wave function in the $(S_j^\dagger)^N|0\rangle$ subspace. For non-S pairs, we diagonalize the H in $(S_j^\dagger)^{N-1}A^{r\dagger}_{j_1j_2}|0\rangle$ space ($A^{r\dagger}_{j_1j_2}$ is the non-S pair with spin $r \neq 0$), with j_1 and j_2 running over all single-particle levels. The structure coefficients of corresponding non-S pairs are obtained based on the energetically lowest eigenstates. Here we consider two types of G pairs with the lowest energy in order to reproduce well the second 4^+ states of even-even nuclei.

The Hamiltonian in this paper includes the spherical single-particle energy term H_0, the residual monopole pairing interaction H_{P0}, the residual quadrupole pairing interaction H_{P2} and the quadrupole-quadrupole interaction H_Q:

$$H = H_0 + H_{P0} + H_{P2} + H_Q, \tag{2}$$

with

$$\begin{aligned} H_0 &= \sum_j \epsilon_j C_j^\dagger C_j, \\ H_{P0} &= -G_0 \mathcal{P}^{(0)\dagger} \cdot \mathcal{P}^{(0)}, \\ H_{P2} &= -G_2 \mathcal{P}^{(2)\dagger} \cdot \mathcal{P}^{(2)}, \\ H_Q &= -\kappa Q \cdot Q, \end{aligned}$$

where ϵ_j is the single-particle energy, G_0, G_2, κ are the two-body interaction parameters of monopole, quadrupole pairing, and quadrupole-quadrupole interactions between valence nucleons (valence neutrons for $Z = 50$ isotopes and valence protons for $N = 82$ isotones). In this paper these two-body parameters are assumed to be unified and are taken as $G_0 = 0.19$, $G_2 = 0.025$, $\kappa = 0.041$ to reproduce the experimental spectra of of yrast states. The pairing operators and quadrupole operators are defined as follows:

$$\begin{aligned} \mathcal{P}^{(0)\dagger} &= \sum_j \frac{\sqrt{2j+1}}{2} (C_j^\dagger \times C_j^\dagger)_0^{(0)}, \\ \mathcal{P}^{(2)\dagger} &= \sum_{jj'} q(jj')(C_j^\dagger \times C_{j'}^\dagger)_M^{(2)}, \\ Q &= \sum_{jj'} q(jj')(C_j^\dagger \times \tilde{C}_{j'})_M^{(2)}, \end{aligned}$$

where $q(jj') = \frac{(-)^{j+1/2}}{\sqrt{20\pi}} \hat{j}\hat{j}' C^{20}_{j\frac{1}{2},j'-\frac{1}{2}} \langle nl|r^2|nl'\rangle$.

The single-particle energies in our calculations are presented in Table I. The neutron single-particle energies of the $g_{7/2}$ and $d_{5/2}$ levels for Sn isotopes are taken as experimental excitation energies of ^{101}Sn, while other single-particle orbits are adopted from a previous shell model calculation [9] as in Ref. [22]. For $N = 82$ isotones with $Z \leqslant 60$, the proton single-particle energies are extracted from the experimental data of ^{133}Sb [53], except that the unmeasured $\epsilon_{s1/2}$ is taken from Ref. [54].

TABLE I. Single-particle energies ϵ_j (in MeV) for $Z = 50$ isotopes (taken from Refs. [22,53]) and $N = 82$ isotones (taken from Refs. [53,54]). The single-particle energy of the $d_{5/2}$ is adjusted in a simple manner for $N = 82$ isotones with proton number $Z = 62$ and 64, as explained in the text.

	$\epsilon_{s_{1/2}}$	$\epsilon_{d_{3/2}}$	$\epsilon_{d_{5/2}}$	$\epsilon_{g_{7/2}}$	$\epsilon_{h_{11/2}}$
$Z = 50$	1.550	1.660	0.000	0.172	3.550
$N = 82$	2.990	2.440	0.962	0.000	2.792

It is worthwhile to discuss the mechanism of the difference between the proton and neutron single-particle energies in Table I. For this purpose, we present here a schematic picture based on the difference of inert cores for Sn isotopes and the $N = 82$ isotones, in Fig. 1, where the energy difference between the single-particle energies of valence protons for $N = 82$ isotones and those of valence neutrons for Sn isotopes is attributed to the proton-neutron interaction between the valence protons and the extra part of neutron core in the $N = 82$ isotones. To see this more clearly, we adopt the proton-neutron part of a monopole-optimized effective interaction for Sn isotopes [55] [denoted by $V_J(j_\pi j_\nu, j_\pi j_\nu)$], and calculate its monopole contribution to the shift of single-particle energy, given by

$$\Delta\epsilon_{j_\pi} = \frac{\sum_{j_\nu,J}(2J+1)V_J(j_\pi j_\nu, j_\pi j_\nu)}{2j_\pi + 1} \tag{3}$$

with j_π the valence-proton level and j_ν running over the extra inert-neutron levels, $\{s_{1/2}, d_{3/2}, d_{5/2}, g_{7/2}, h_{11/2}\}$, of the $N = 82$ isotones. The resultant values are $\Delta\epsilon_{g_{7/2}} = -2.3$ MeV

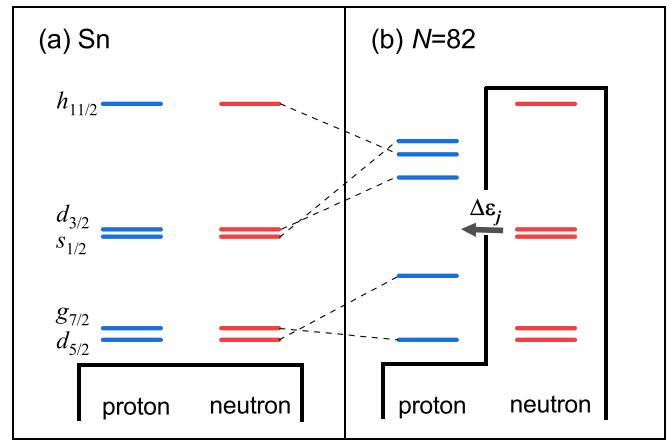

FIG. 1. Schematic picture of difference between the single-particle energies of valence protons for $N = 82$ isotones and those of valence neutrons for Sn isotopes, based on the proton-neutron interaction between the valence protons and the extra part of neutron core in the $N = 82$ isotones. See the text for details.

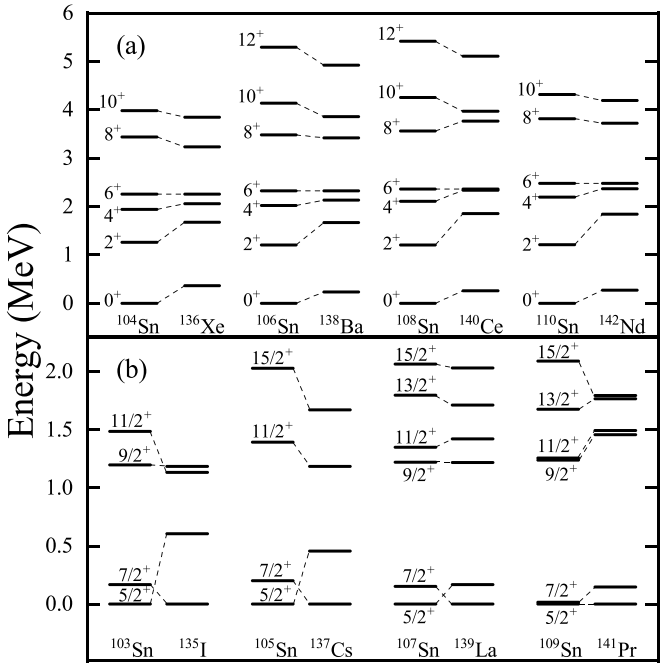

FIG. 2. Comparison of the experimental yrast states for (a) even-even $^{104–110}$Sn and ^{136}Xe – ^{142}Nd, and (b) odd-mass $^{103–109}$Sn and ^{135}I – ^{141}Pr. For convenience of comparison, the levels of even-even $N = 82$ isotones are shifted to put the 6^+ states at the same place as their partners in Sn isotopes. The experimental excitation energies were taken from Ref. [53].

and $\Delta\epsilon_{d_{5/2}} = -1.6$ MeV. This means that the proton $g_{7/2}$ level should be lowered down by about 0.7 MeV, and become the lowest single-particle level for $N = 82$ isotones. In Table I, the change of $\epsilon_{g_{7/2}}$ from neutron to proton is about 1.1 MeV, slightly larger than the theoretical estimation. We note the single-particle energies of these two levels used in Ref. [55] are reversed in comparison to the experimental data, which could account appropriately for this discrepancy.

For electromagnetic properties, we take the effective charges as $e_\nu = 1.28\,e$ for neutron systems and $e_\pi = 1.60\,e$ for proton systems; the effective gyromagnetic ratios are optimized to be $g_{l\nu} = -0.01\,\mu_N$, $g_{s\nu} = -3.826 \times 0.7\,\mu_N$ for neutron systems, and $g_{l\pi} = 1.10\,\mu_N$, $g_{s\pi} = 5.586 \times 0.7\,\mu_N$ for proton systems, respectively.

III. RESULTS AND DISCUSSION

In this section we present our calculated results of low-lying states for the Sn isotopes and the $N = 82$ isotones. All effective parameters in the NSM and NPA calculations are presented in the preceding section. Based on these results we discuss the nice symmetry manifested in the even-even nuclei, and investigate the origin for the large differences of 2_1^+ energies therein.

A. Symmetry between corresponding valence mirror nuclei

In Fig. 2 we plot experimental energy levels for yrast states of the $Z = 50$ isotopes, $^{103–110}$Sn, and $N = 82$ isotones, ^{135}I – ^{142}Nd, taken from the National Nuclear Data Center (NNDC) [53]. For convenience, to compare the relative energy intervals, we shift the levels of ^{136}Xe, ^{138}Ba, ^{140}Ce, and ^{142}Nd so that the 6_1^+ states of the $N = 82$ isotones locate at the "same level" as the corresponding Sn isotopes. We have chosen the 6_1^+ state as a reference because this state has a quite pure $|S^n I\rangle$ configuration in the investigated nuclei. One sees that the yrast states with $J = 4$–12 for those even-even Sn isotopes and the $N = 82$ isotones have nice one-to-one correspondences, with level schemes very close to each other, except for the energies of the 2_1^+ states. This similarity in energy spectra and the asymmetry in 2_1^+ states were noted already in Refs. [2–5]. In addition, such a level symmetry totally breaks down in the odd-mass nuclei, as shown by the mismatch of the order of $\frac{7}{2}_1^+$ and $\frac{5}{2}_1^+$ levels in particular. This is because in the seniority picture these yrast states are dominantly controlled by the unpaired nucleon, and accordingly they are very sensitive to the single-particle energy splittings. The asymmetry presented in the 2_1^+ states will be discussed in the next subsection.

Figure 3 plots both the NSM and the NPA results for the low-lying energy spectra of even-even $^{102–110}$Sn and ^{134}Te – ^{142}Nd. The experimental data available in the NNDC are also exhibited for comparison. One sees that the yrast levels from the NPA calculation are well consistent with experimental values as well as the corresponding NSM results. Most importantly, the remarkable similarities between Sn isotopes and and $N = 82$ isotones are reproduced very well.

One attractive feature in that figure is the similarity of energy levels between non-yrast positive-parity states. In experimental data, we find that the non-yrast states energies of 0_2^+, 2_2^+, 4_2^+, 6_2^+ are 2.31, 2.12, 2.46, 2.75 MeV for ^{110}Sn, and 2.22, 2.38, 2.44, 2.89 MeV for ^{142}Nd. From theoretical calculations, this feature is distinctly indicated by the semidegeneracies of 0^+-6^+, 7^+-8^+, and 9^+-10^+ states in the NSM results. Such a behavior is also reproduced by the NPA calculation for ^{140}Ce, ^{110}Sn, and ^{142}Nd, although the exact level orders are not consistent with the NSM results. It thus provides a guidance for future experimental measurements related to the proton-rich Sn isotopes, for which relevant experimental data connecting the valence mirror symmetry are rare.

The negative-parity levels of our NSM and NPA calculations, however, are not well consistent with the experimental data. According to Ref. [56], the agreement is improved by further considering octupole pairing and octupole-octupole interaction in the phenomenological Hamiltonian, and the symmetry for the negative-parity levels broken in our calculations is also recovered partially by the incorporation of appropriate octupole interactions.

Figure 4 shows the theoretical and experimental results of low-lying states for the odd-mass Sn isotopes and $N = 82$ isotones. The calculated positive-parity levels among the NSM, the NPA, and the experimental results are in good agreement, except that the ground state of ^{109}Sn is not reproduced by the theoretical calculations. For negative-parity states, the NSM and the NPA results are consistent with each other, but not consistent with experimental data. Such deviations may be partly attributed to the absence of monopole interactions; for

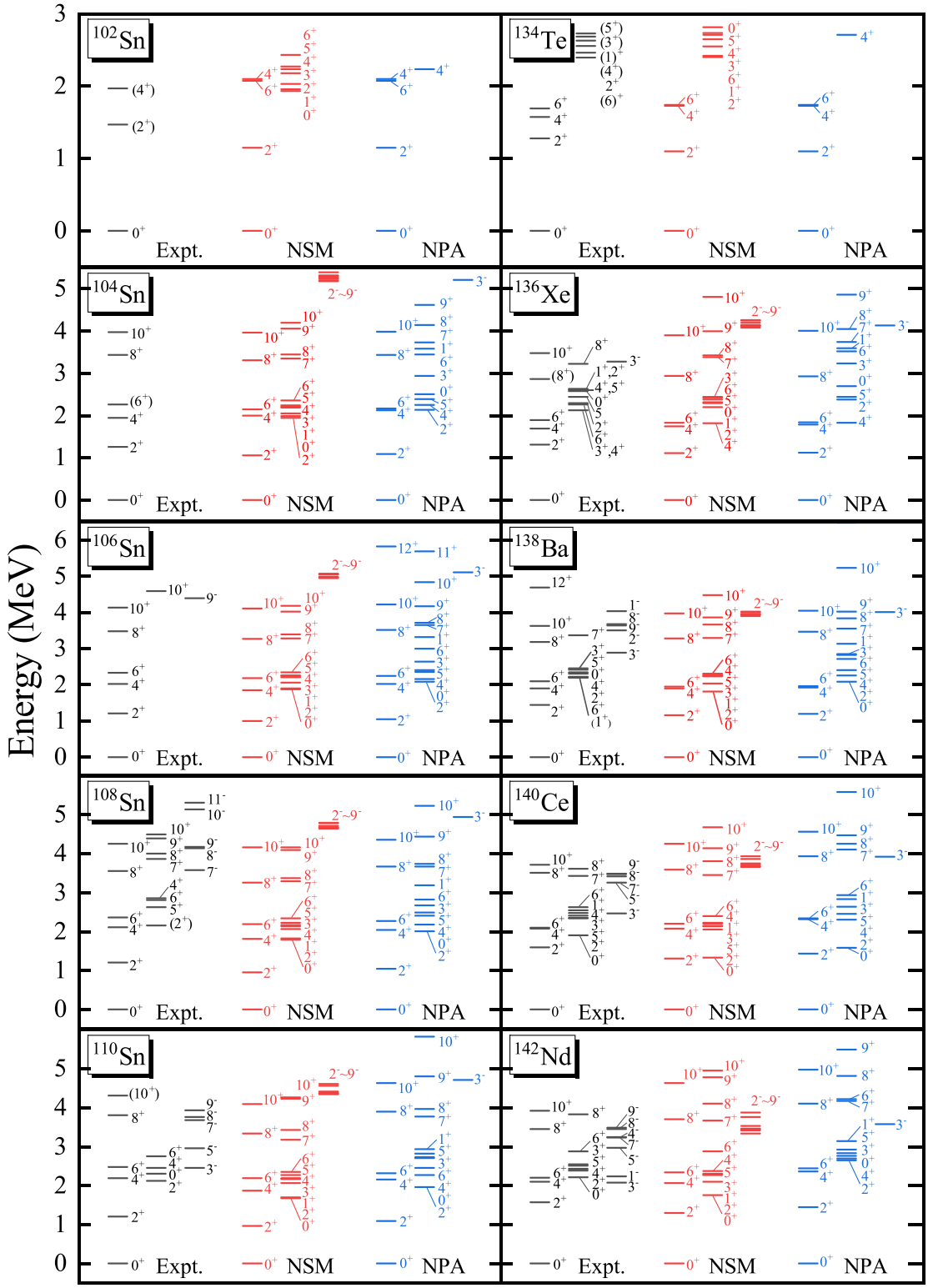

FIG. 3. Low-lying energy spectra for even-even $^{102-110}$Sn and ^{134}Te – ^{142}Ba. Experimental data from the NNDC database [53] are plotted in black. The shell model results (in red) and the NPA results (in blue) are obtained by diagonalizing the phenomenological pairing plus quadrupole-quadrupole interaction.

instance, the introduction of $G\sum_{JM}(C^{\dagger}_{5/2}\times C^{\dagger}_{11/2})^{(J)}_{M}(\tilde{C}_{5/2}\times \tilde{C}_{11/2})^{(J)}_{M}$ with $G = 0.4$ MeV reduces the excitation energies of $\frac{11}{2}^{-}_{1}$ states in ^{107,109}Sn from 2.61 and 2.31 MeV to 1.70 and 1.15 MeV, respectively, close to 1.67 and 1.27 MeV measured in experiments. Note that this monopole interaction has very slight contribution to the positive-parity levels. Nonetheless, the valence mirror symmetry for the odd-mass nuclei is not

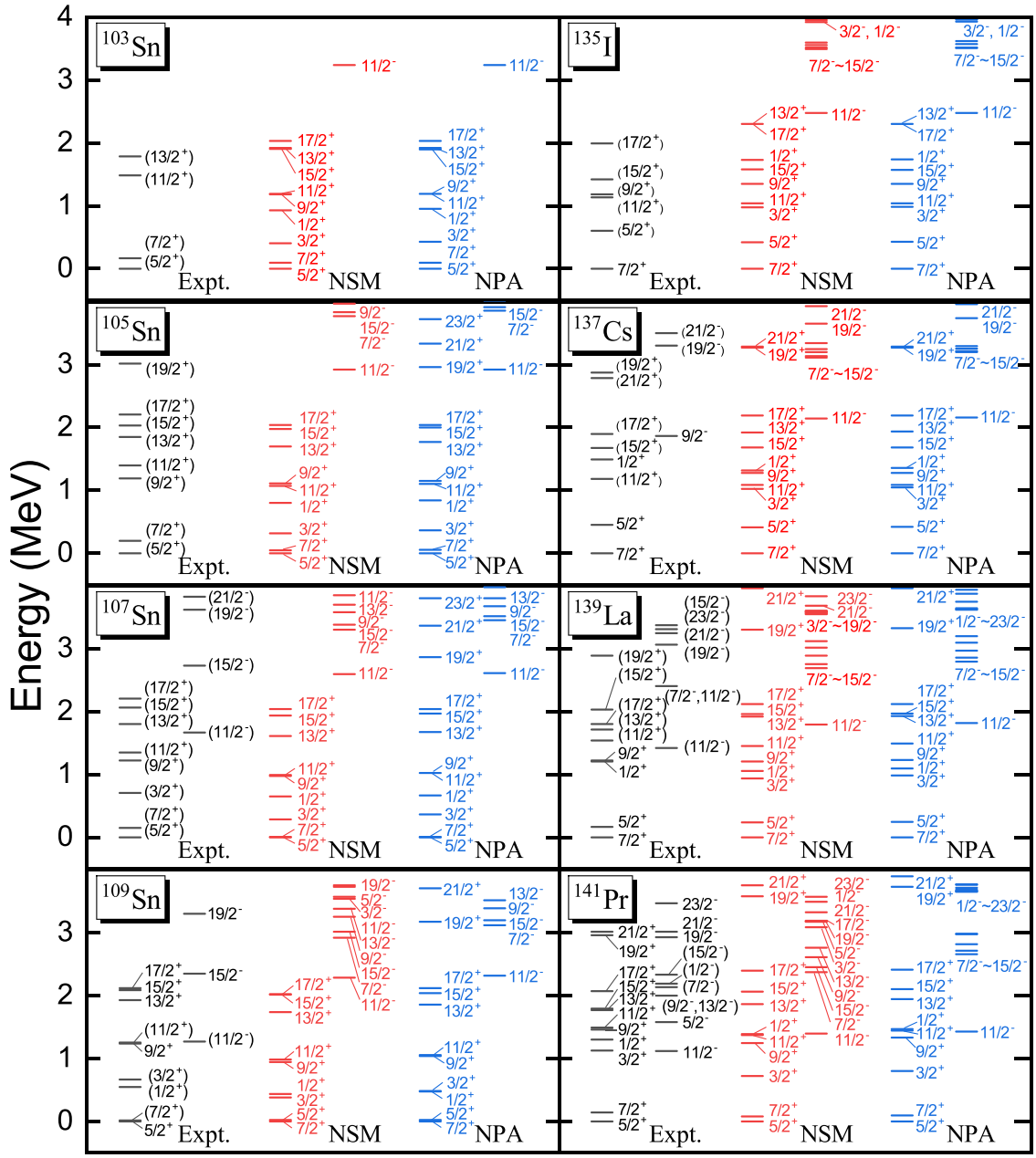

FIG. 4. Same as Fig. 3, but for even-odd $^{103-109}$Sn and odd-even ^{135}I – ^{141}Pr.

clearly seen, either experimentally or theoretically. Therefore below we focus our discussion on valence mirror symmetry in the even-even nuclei.

As studied in Refs. [2–5], the simplest explanation of the valence mirror symmetry would be the identical single-particle energies and residual interactions for valence nucleons outside magic cores. Here we also adopt the identical two-body interaction parameters for valence mirror nuclei with the same valence nucleon numbers (but take different single-particle energies). In order to investigate the valence mirror symmetry, we compare the NPA wave functions of the corresponding states connected by this symmetry, by neglecting the isospin part of wave functions for valence protons and neutrons. The overlaps between wave functions of relevant states for the Sn isotopes and the corresponding wave functions for the $N = 82$ isotones are calculated, and plotted in panels (a)–(c) of Fig. 5, respectively, where n represents the number of valence nucleons. One sees that most of those calculated overlaps are larger than 0.8, which demonstrate notable similarities between corresponding states and thus the existence of nice valence mirror symmetry for the Sn isotopes and the $N = 82$ isotones. An interesting feature is that the overlaps for non-yrast states are in general larger than for yrast states, consistent with the tendency seen in Figs. 3 and 4.

Now we look at the electromagnetic properties of these nuclei. In Table II, we list the calculated values of $B(E2)$ (in units of W.u.) for the yrast states of the even-even $^{102-110}$Sn and ^{134}Te – ^{142}Nd, as well as corresponding experimental data

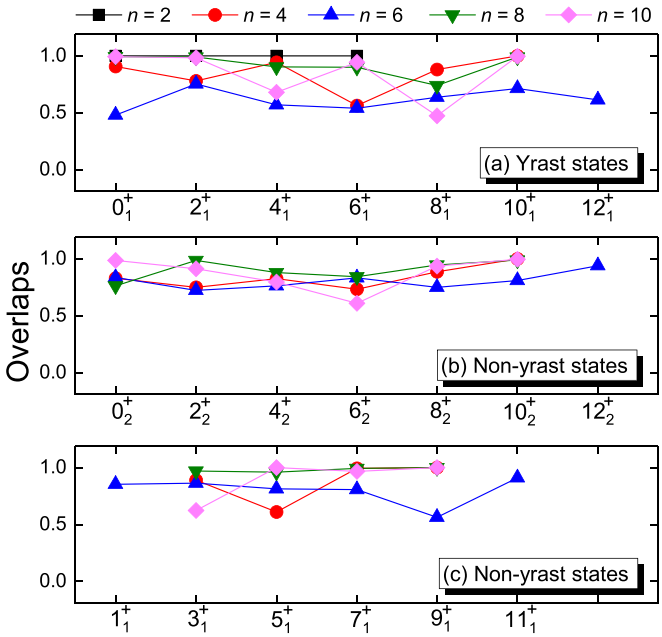

FIG. 5. Overlaps of the NPA wave functions for states of the Sn isotopes with those for corresponding states of the $N = 82$ isotones, versus valence nucleon number n. Panels (a)–(c) correspond to the yrast states and the non-yrast states with even J and odd J, respectively.

for comparison [53,57]. One sees that the NPA calculations are well consistent with the NSM results, whereas they are in visible disagreement with some experimental data. These discrepancies primarily result from the simple form for residual interaction adopted in this work. In Refs. [23,34], more complicated interactions were applied to the NPA calculations and yielded a relatively better agreement for the considered $B(E2)$ values. There are also a few states of the $N = 82$ isotones that are experimentally known to have quadrupole moments [53]: $-0.14(7)\,eb$ for the 2_1^+ state of ^{138}Ba; 0.35(7) and 0.34(4) eb for the 4_1^+ and 6_1^+ states of ^{140}Ce. In the NPA calculations, we obtain -0.294, -0.062 and 0.127 eb for these three states; in the NSM calculations, the corresponding values are -0.327, -0.037 and 0.167 eb. Nevertheless, the phenomenological pairing plus quadrupole-quadrupole interaction adopted in this work describes the bulk properties of the examined nuclei well.

Magnetic dipole moment is a sensitive probe for nuclear structures. We have also derived this quantity from the NSM and the NPA calculations, and present it together with data available from the NNDC in Table III. For $N = 82$ isotones, the NSM and the NPA results are well consistent with each other and the experiments. For Sn isotopes, however, the experimental data are still scarce and subject to large uncertainties, and our calculations reproduce the general feature exhibited in these experimental magnetic moments. Yet the differences among the NSM, the NPA, and the experiments are discernible, although the present calculations yield $\mu(6_1^+)$ for ^{108}Sn, close to the shell model value based on a more sophisticated Hamiltonian [23]. More experimental measurements of magnetic moments and calculations with a sophisticated Hamiltonian in larger configuration spaces are thus warranted.

TABLE II. $B(E2; I \to I-2)$ (in units of W.u.) for yrast states of even-even $^{102-110}$Sn and ^{134}Te – ^{142}Nd. Experimental data are taken from Ref. [53]. The neutron effective charge is taken to be $e_\nu = 1.28\,e$, while the proton effective charge is taken to be $e_\pi = 1.60\,e$.

	^{102}Sn			^{134}Te		
I^π	Expt.	NSM	NPA	Expt.	NSM	NPA
2_1^+		5.24	5.24	6.3(20)	5.09	5.09
4_1^+		2.06	2.06	4.3(4)	4.04	4.04
6_1^+		0.45	0.45	2.05(4)	2.24	2.24
	^{104}Sn			^{136}Xe		
	Expt.	NSM	NPA	Expt.	NSM	NPA
2_1^+	11.9(19)	9.95	9.59	9.68(38)	8.42	7.84
4_1^+		10.6	8.85	1.281(17)	6.16	5.90
6_1^+	4.2(15)	0.31	0.67	0.0132(4)	3.95	4.04
8_1^+	>0.6	3.09	3.68		4.14	4.07
10_1^+	4.1(6)	5.22	3.15		0.30	0.21
	^{106}Sn			^{138}Ba		
	Expt.	NSM	NPA	Expt.	NSM	NPA
2_1^+	13.1(26)	13.4	12.8	10.8(5)	9.75	9.13
4_1^+		17.9	15.9	0.2873(15)	4.08	3.80
6_1^+	3.1(7)	0.76	0.94	0.053(7)	1.33	1.15
8_1^+		1.93	4.06		0.17	0.19
10_1^+	6.4(11)	0.40	0.08	1.59(22)	3.31	3.24
	^{108}Sn			^{140}Ce		
	Expt.	NSM	NPA	Expt.	NSM	NPA
2_1^+	14.5(12)	15.4	14.8	13.8(3)	12.2	12.0
4_1^+		21.8	20.1	0.137(4)	5.18	5.43
6_1^+	2.43(14)	0.29	0.42	0.29(6)	0.25	0.18
8_1^+		5.67	5.70		1.35	0.41
10_1^+		0.52	0.53	0.46(13)	4.02	3.75
	^{110}Sn			^{142}Nd		
	Expt.	NSM	NPA	Expt.	NSM	NPA
2_1^+		15.9	15.7	12.03(22)	14.5	15.4
4_1^+		23.1	20.8		6.53	3.24
6_1^+		0.09	0.04		0.20	0.13
8_1^+		6.25	5.44		6.18	6.26
10_1^+		1.16	1.37		0.86	0.67

For one pair of mirror nuclei, the similarity of nuclear structures leads to exact symmetry in electromagnetic properties: the magnetic moments of mirror nuclei exhibit strong linear correlations for both the ground and excited states [58]. This pattern might be expected to survive for valence mirror nuclei. However, magnetic moments in Table III do not follow this regularity. In order to investigate the reason why this correlation disappears for one pair of valence mirror nuclei, we calculate the reduced matrix elements of magnetic moments in Fig. 6 for yrast states with given spin J. The calculated $\xi_l = \langle\Psi||L||\Psi\rangle$ and $\xi_s = \langle\Psi||S||\Psi\rangle$, with $|\Psi\rangle$ the NPA wave function, are plotted by using squares and circles,

TABLE III. Same as Table II, but for magnetic moment μ (in units of μ_N). Experimental data are taken from Ref. [53]. The neutron gyromagnetic ratios are optimized to be $g_{l\nu} = -0.01\,\mu_N$ and $g_{s\nu} = -3.826 \times 0.7\,\mu_N$, while the proton gyromagnetic ratios are taken to be $g_{l\pi} = 1.10\,\mu_N$ and $g_{s\pi} = 5.586 \times 0.7\,\mu_N$.

	^{102}Sn			^{134}Te		
I^π	Expt.	NSM	NPA	Expt.	NSM	NPA
2_1^+		−0.16	−0.16		1.67	1.67
4_1^+		−1.96	−1.96		3.15	3.15
6_1^+		−0.30	−0.30	5.08(15)	4.74	4.74
	^{104}Sn			^{136}Xe		
	Expt.	NSM	NPA	Expt.	NSM	NPA
2_1^+		−0.07	−0.06	1.53(9)	1.71	1.68
4_1^+		−0.13	−0.27	3.2(6)	3.14	3.15
6_1^+		−0.23	−0.27		4.74	4.74
8_1^+		0.41	−0.33		6.37	6.37
10_1^+		−0.28	−0.28		10.1	10.1
	^{106}Sn			^{138}Ba		
	Expt.	NSM	NPA	Expt.	NSM	NPA
2_1^+		−0.03	−0.01	1.44(22)	1.76	1.74
4_1^+		−0.03	−0.03	3.2(6)	3.20	3.19
6_1^+	−0.84(54)	−0.16	−0.20	5.88(12)	4.77	4.78
8_1^+		0.46	−0.07		8.43	8.43
10_1^+		−0.09	−0.22		10.1	10.1
	^{108}Sn			^{140}Ce		
	Expt.	NSM	NPA	Expt.	NSM	NPA
2_1^+		−0.01	0.01	1.9(2)	2.07	2.05
4_1^+		0.09	0.11	4.06(15)	3.92	3.87
6_1^+	−0.24(12)	−0.06	0.08		6.62	6.83
8_1^+		0.41	0.18		7.88	7.89
10_1^+		0.28	0.18	10.3(4)	11.3	11.4
	^{110}Sn			^{142}Nd		
	Expt.	NSM	NPA	Expt.	NSM	NPA
2_1^+	0.58(22)	0.01	0.05	1.69(15)	2.48	2.40
4_1^+	0.20(56)	0.04	0.14		5.76	6.14
6_1^+	0.06(114)	−0.00	0.32		6.80	6.86
8_1^+		0.09	0.31		9.48	9.43
10_1^+		0.42	0.53	7.9(24)	11.3	11.4

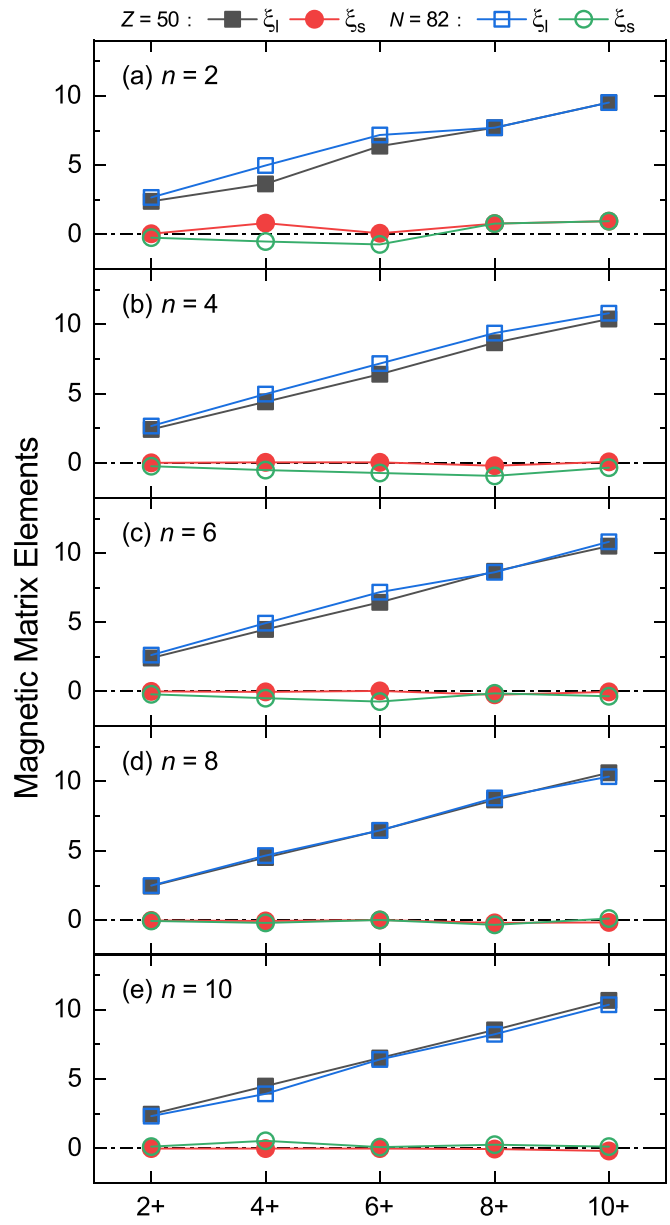

FIG. 6. Matrix elements of magnetic dipole moment for the yrast states of even-even Sn isotopes (in black and red) and those of $N = 82$ isotones (in blue and green), with the valence nucleon number $n = 2$–10. The orbital parts (ξ_l) and spin parts (ξ_s) are represented by using squares and circles, respectively.

respectively. Panels (a)–(e) correspond to cases with valence nucleon numbers $n = 2$, 4, 6, 8, and 10 respectively, with results of the Sn isotopes in black and red and those of the $N = 82$ isotones in blue and green. According to Fig. 6, the dominant contributions to the total magnetic moments come from the orbital angular momentum parts, while those from spin parts are very small. Very strikingly, it is easily seen that the magnetic moments of corresponding states for given pair of valence mirror nuclei, given by orbital angular momentum parts, are close to each other, and are approximately proportional to J. This means that the asymmetry in magnetic moments essentially originates from the difference in gyromagnetic ratios for valence protons and neutrons ($g_{l\nu} = -0.01\,\mu_N$ and $g_{l\pi} = 1.10\,\mu_N$ in this paper).

A simple scenario of the regular pattern for ξ_l can be understood in the framework of the NPA by two steps. First let us look at the case of two identical nucleons, in which case the matrix element of magnetic moments is already derived in Ref. [52] as follows:

$$\langle s_1, J_1' \| L \| r_1, J_1 \rangle = (-)^t \delta_{s_1,r_1'} \delta_{J_1',L_1} \langle s_1, J_1' | \mathbf{r}_1', L_1 \rangle,$$
$$= (-)^t \delta_{s_1,r_1'} \sum_{jj'} 2y(jj's_1) y'(j'jr_1'), \quad (4)$$

where $y(jj's_1)$ is the structure coefficient, and $\mathbf{r}'_1$ represents a new collective pair,

$$\mathbf{r}'_1 \equiv A_M^{r'_1\dagger} = \sum_{jj'} y(jj'r'_1)(C_j^\dagger \times C_{j'}^\dagger)_M^{r\dagger}, \tag{5}$$

where $y'(j'jr'_1)$ is defined as

$$y'(j'jr'_1) = z(j'jr'_1) - \theta(j'jr'_1)z(jj'r'_1), \tag{6}$$

$$z(j'jr'_1) = \sqrt{3}\hat{r}_1 \sum_k y(jkr_1)q(kj'1)\begin{Bmatrix} r_1 & 1 & r'_1 \\ j' & j & k \end{Bmatrix}, \tag{7}$$

with $\theta(j'jr'_1) = (-)^{j'+j+r'_1}$ and

$$q(jj'1) = \delta_{ll'}(-1)^{l+1/2+j'}\sqrt{\frac{l(l+1)}{3}}\hat{j}\hat{j}'\hat{l}\begin{Bmatrix} j & j' & 1 \\ l & l & \frac{1}{2} \end{Bmatrix} \tag{8}$$

the structure coefficient of the operator L. The absolute values of nondiagonal elements in $q_l(jj'1)$ are very small compared with the diagonal elements. By assuming that $q(jj'1) = 0$ when $j \neq j'$, $y'(j'jr'_1)$ in orbital parts is reduced to

$$y'(j'jr'_1) = y(jj'r_1)f(j'jr_1), \tag{9}$$

with

$$\begin{aligned} f(j'jr_1) = \hat{r}_1\Bigg((-1)^{l'+1/2+j'}&\sqrt{l'(l'+1)}(2j'+1)\hat{l}' \\ &\times \begin{Bmatrix} l' & l' & 1 \\ j' & j' & \frac{1}{2} \end{Bmatrix}\begin{Bmatrix} r_1 & r_1 & 1 \\ j' & j' & j \end{Bmatrix} \\ &+ (-1)^{l+1/2+j}\sqrt{l(l+1)}(2j+1)\hat{l} \\ &\times \begin{Bmatrix} l & l & 1 \\ j & j & \frac{1}{2} \end{Bmatrix}\begin{Bmatrix} r_1 & r_1 & 1 \\ j & j & j' \end{Bmatrix}\Bigg). \end{aligned} \tag{10}$$

Empirically, by many numerical experiments, we find an approximate identity: the function inside the bracket of the right hand side in the above equation equals -1 in very high precision, regardless of l, l', j, j', or r_1. Substituting all these results in Eq. (4), one obtains

$$\langle s_1, J'_1 \| L \| r_1, J_1 \rangle \simeq \delta_{J'_1,J_1}\delta_{s_1,J'_1}\delta_{r_1,J_1}J_1. \tag{11}$$

This means that for $n = 2$ the matrix elements of L are approximately given by J_1. The second step of the scenario is that the above comments for the $n = 2$ case are also applicable for $n > 2$. This is readily known for the single-j case. In Ref. [59], Talmi pointed out that, in the single-j orbit, only non-S pairs contributed to the magnetic moments in a many-particle system. In the NPA calculations, the yrast low-lying states of semimagic even-even nuclei are well described by the optimized pair basis states, most of which are generalized seniority-2 states [23,34]. In the yrast states of nuclei with $n > 2$, similar to the single-j case, only one non-S pair contributes to the magnetic moments. As a result, the orbital parts in Fig. 6 take almost the same values for nuclei with $n > 2$ as those with $n = 2$. As low-lying states of even-even $N = 82$ isotopes are dominated by a configuration of one broken proton pair, for which the magnetic moments are essentially given by the orbital part, the simple pattern of magnetic moments discussed here is expected to be very useful to predict the magnetic moments of those neutron-rich even-even $N = 82$ isotopes for which experimental results of magnetic moments are not yet available. We note without details that this simple pattern is well consistent with other calculations in the shell model and interacting boson model [26,60].

B. Asymmetry for the 2_1^+ states

In the above subsection, we demonstrate the symmetric aspects of the corresponding valence mirror nuclei, the Sn isotopes and $N = 82$ isotones. In this subsection, we come to the asymmetric aspect, and try to interpret the most interesting behavior related to the 2_1^+ states of corresponding valence mirror nuclei. In Refs. [2–5], it was suggested that core excitations are responsible for energy difference between the valence mirror 2_1^+ states. Here we revisit this issue, and suggest an alternative, i.e., this asymmetry is simply given by different single-particle energies of corresponding valence mirror nuclei.

As indicated by the calculated $E_{2_1^+}$, $B(E2; 2_1^+ \to 0_1^+)$, and $\mu(2_1^+)$ in respectively Fig. 3 and Tables II and III, the NPA can exactly reproduce the 2_1^+ state in the shell-model valence space. Therefore in this subsection we adopt the NPA and use it to calculate $E_{2_1^+}$ of the systems towards the half-filled shell. The configuration space for these 2_1^+ states is constructed from S pairs and one D pair for simplicity. There are also previous studies showing the appropriateness of this subspace for the estimation of properties such as $E_{2_1^+}$, $B(E2)$, and magnetic moments [21,22]. The Hamiltonian is same as the one we used in the preceding subsection.

Here, we investigate the evolution of $E_{2_1^+}$ versus valence nucleon number n, for both Sn isotopes and $N = 82$ isotones. For convenience, we take the $E_{2_1^+}$ values with $n = 2$ as the references and plot the difference $\Delta E_{2_1^+}$ in Fig. 7. Results from the NPA and other theoretical calculations [9,30,31] are also shown for comparison. One sees that our NPA calculations reproduce the changes of $\Delta E_{2_1^+}$ very well. One also sees that $\Delta E_{2_1^+}$ values of $N = 82$ isotones exhibit a kink at $n = 8$ and a sharp jump at $n = 14$, which are very different from the evolutions of $\Delta E_{2_1^+}$ for Sn isotopes and are related to the shell closure of the $Z = 64$ proton subshell.

In order to understand the origin of these differences, we decompose the NPA results of $\Delta E_{2_1^+}$ into four parts corresponding to the single-particle, monopole-pairing, quadrupole-pairing, and quadrupole-quadrupole terms in the Hamiltonian, and plot the evolution of these contributions versus n in Fig. 8. It is easy to see that $\Delta E_{2_1^+}$ versus n for the single-particle term of $N = 82$ isotones changes more significantly than that of Sn isotopes, while the changes of other terms versus n are very close to each other for these corresponding valence mirror nuclei. This shows that the asymmetry for 2_1^+ state energies is essentially given by the single-particle energy term.

It is therefore necessary to look more closely at the single-particle energies ϵ_j individually for $N = 82$ isotones and Sn isotopes. For $N = 82$ isotones with $52 \leqslant Z \leqslant 60$, our single-particle energies are fixed as the values listed in Table I. For those with $Z = 62$ and 64, $\epsilon_{2d_{5/2}}$ is assumed to decrease smoothly to reflect the subshell closure. Namely, the energy

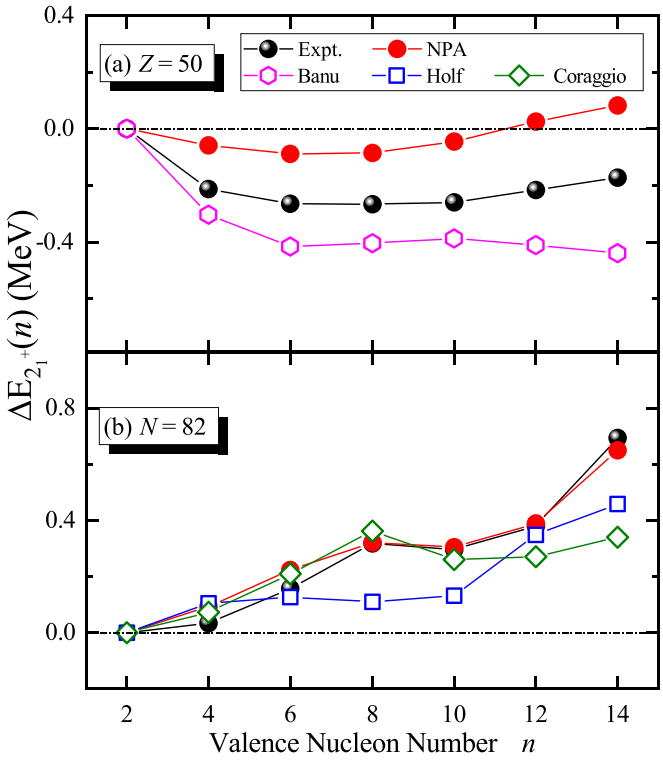

FIG. 7. $\Delta E_{2_1^+}(n)$ versus valence nucleon number n, for even-even $Z = 50$ isotopes (a) and $N = 82$ isotones (b). Experimental data are extracted from Ref. [53]. Other theoretical results of Refs. [9,30,31] are included for comparison.

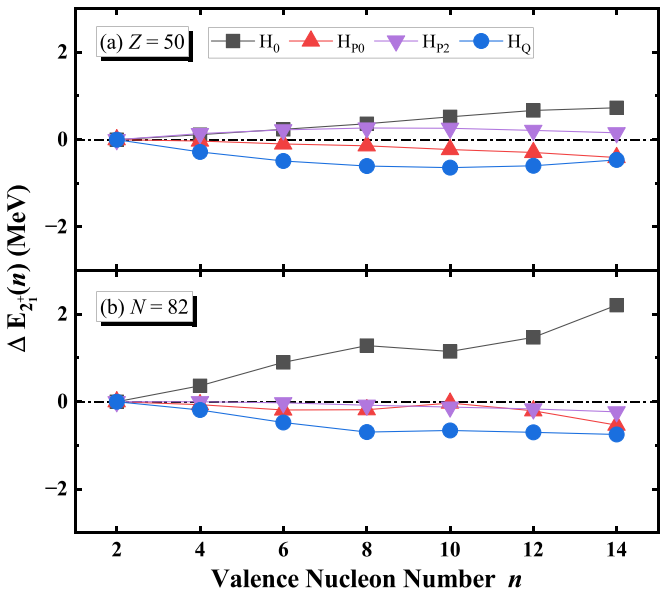

FIG. 8. Evolution of various interaction terms (denoted by H_0, H_{P0}, H_{P2}, and H_Q) in the 2_1^+ state with respect to cases of two-nucleon systems, denoted by ΔE for short, for the Sn isotopes and $N = 82$ isotones, versus valence particle number n. H_0 corresponds to the single-particle energy term, H_{P0} and H_{P2} correspond to monopole and quadrupole pairing interactions, and H_Q corresponds to the quadrupole-quadrupole interaction. Panels (a) and (b) correspond to $Z = 50$ isotopes $N = 82$ isotones, respectively.

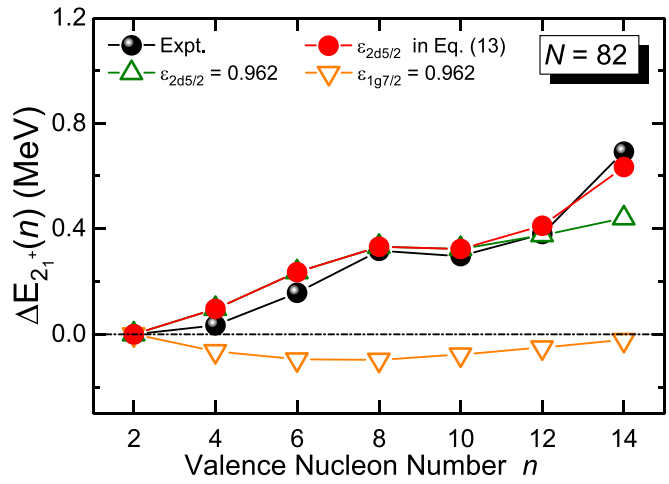

FIG. 9. $\Delta E_{2_1^+}$ (in MeV) versus valence nucleon number n, for even-even $N = 82$ isotones calculated with different $\epsilon_{2d_{5/2}}$ and $\epsilon_{1g_{7/2}}$. $\Delta E_{2_1^+}$ extracted from experimental data are represented by solid circles in black. Solid circles in red correspond to calculated results with $\epsilon_{2d_{5/2}}$ of Eq. (12). Open triangles in olive correspond to calculated results with fixed value of $\epsilon_{2d_{5/2}}$ in Table I. Inverted triangles in orange correspond to calculated results with the $g_{7/2}$ orbit artificially upshifted by 0.962 MeV and degenerate with the $d_{5/2}$ orbit.

difference between $2d_{5/2}$ and $1g_{7/2}$ (denoted by $\Delta\epsilon = \epsilon_{2d_{5/2}} - \epsilon_{1g_{7/2}}$) is significantly reduced around ^{146}Gd [61]: the $\Delta\epsilon$ value decreases from ≈1.0 to ≈0.4 MeV. For completeness, here we refer to works regarding this subshell: The emergence of subshell closure $Z = 64$ and the shell quenching near the neutron-drip line in $N = 82$ isotones have been studied both theoretically and experimentally [61–66]. In Ref. [62], the study of high-spin isomers along $N = 82$ isotones suggested that the subshell gap of $Z = 64$ increased from 2.0 to 2.4 MeV as the number of valence protons increased from 11 to 15. In the relativistic mean-field approaches, the relativistic Hartree-Fock theory well described the Z dependence of $\Delta\epsilon$ values after including the nonlocal exchange terms, and indicated that the value of $\Delta\epsilon$ decreases roughly by half as the number of valence protons increased from 8 to 14 [63]. The shell model calculations in Refs. [67,68] also employed small $\Delta\epsilon$ values for the $N = 82$ isotones around ^{164}Gd, with $\Delta\epsilon$ equaling 0.6 MeV and 0.4 MeV, respectively. By using the experimental results in Ref. [61], we obtain the optimized value of $\epsilon_{2d_{5/2}}$(in unit of MeV) as follows:

$$\epsilon_{2d_{5/2}} = \begin{cases} 0.962, & n \leqslant 10, \\ 0.962 - 0.137(n-10), & 10 < n \leqslant 14, \end{cases} \quad (12)$$

where n is the valence proton number. Namely, $\epsilon_{2d_{5/2}} = 0.962$ MeV for $n \leqslant 10$ and $\epsilon_{2d_{5/2}} = 0.414$ MeV when $n = 14$. This lowering of the $2d_{5/2}$ single-particle level leads to a pronounced subshell closure at proton number $Z = 64$.

The sharp increase of $\Delta E_{2_1^+}$ in $N = 82$ isotones is highly related to the single-particle energies and in particular the subshell at $Z = 64$. Figure 9 shows the theoretical $\Delta E_{2_1^+}$ of

$N = 82$ isotones calculated with different values of $\epsilon_{2d_{5/2}}$. Solid circles in black represent experimental results, and solid circles in red represent results calculated by the NPA with $\epsilon_{2d_{5/2}}$ of Eq. (12). Open triangles in olive correspond to results calculated with $\epsilon_{2d_{5/2}} = 0.962$ MeV, i.e., the value of Table I; in this case the sudden increase of the calculated $\Delta E_{2_1^+}$ at $n = 14$ would not arise. This means that the subshell closure is responsible for the sudden increase of $E_{2_1^+}$ for the ^{146}Gd nucleus.

We note that the values of single-particle energies for the two orbits, $g_{7/2}$ and $d_{5/2}$, are very important to account for the asymmetry of the $E_{2_1^+}$ of the corresponding valence mirror nuclei. For even-even Sn isotopes, $g_{7/2}$ and $d_{5/2}$ orbits are nearly degenerate, which results in the calculated very small $\Delta E_{2_1^+}$ for the Sn isotopes in this paper, as shown in Fig. 7(a). For even-even $N = 82$ isotones, $\Delta E_{2_1^+}$ increases with n (when $n \leqslant 14$), as shown in Fig. 9(b). We note that the sharp increase of $\Delta E_{2_1^+}$ at $n = 14$ disappears if we artificially require $\epsilon_{2d_{5/2}} = \epsilon_{1g_{7/2}}$ and all other single-particle levels are lowered by 0.962 MeV, namely, we shift up the $1g_{7/2}$ orbit by 0.962 MeV while other single-particle energies are the same as in Table I; note that the inverted open triangles in orange in Fig. 9, are very close to the corresponding results for Sn isotopes given in Fig. 7(a).

Finally we comment on the evolution of the single-particle splitting between the $2d_{5/2}$ and $1g_{7/2}$ orbits, related to the emergence of the $Z = 64$ subshell. A simple picture was provided by Casten in Ref. [4] in terms of the residual neutron-proton interactions between valence protons and neutrons in the 50–82 shell. For $N = 82$ isotones, the $N = 50$–82 shell is closed, and according to Ref. [4] the residual neutron-proton interactions between this closed shell and the open proton shell lowers the proton $1g_{7/2}$ orbit relative to the $2d_{5/2}$ orbit, because the neutron-proton interaction strength of the $1g_{7/2}$ orbit is relatively larger than that of the $2d_{5/2}$ orbit, and furthermore there are more valence neutrons in the $1g_{7/2}$ orbit than in the $2d_{5/2}$ orbit. Thus the residual neutron-proton interactions lead to a larger splitting between the the $2d_{5/2}$ and $1g_{7/2}$ orbits of valence protons for $N = 82$ isotones than that of valence neutrons for Sn isotopes, for which the $2d_{5/2}$-$1g_{7/2}$ splitting is very small. The difference of the $2d_{5/2}$-$1g_{7/2}$ splitting for valence neutrons of even-even Sn isotopes and that for valence protons of the even-even $N = 82$ isotones is necessary to account for the asymmetry in the 2_1^+ states for corresponding valence mirror nuclei studied in this paper.

IV. SUMMARY

In this paper, we study the so-called valence mirror symmetry of low-lying states, for $Z = 50$ isotopes and corresponding $N = 82$ isotones, using both the nuclear shell model (NSM) and its nucleon-pair approximation (NPA). The comparison between the NSM and the NPA results shows that the NPA is essentially valid for the yrast states of both the even-even and odd-mass nuclei considered in this paper. Our calculated energy spectra and electromagnetic properties of low-lying positive-parity states are in good agreement with accessible experimental data. Remarkable correspondences between low-lying states of valence mirror partners with even protons and neutrons are seen, both experimentally and theoretically.

Among a number of features for low-lying states, we study in details the matrix elements of nuclear magnetic moments for yrast states, and find that those matrix elements of even-even Sn isotopes are very close to those of corresponding valence mirror nuclei, namely, $N = 82$ isotones. We provide a simple explanation of this feature in terms of seniority scheme. The simple pattern exhibited in the matrix elements of those valence mirror nuclei are useful in evaluating relevant magnetic moments which are still unavailable in experimental measurements.

We also study in detail the asymmetry for the $E_{2_1^+}$ values of corresponding valence mirror nuclei, and point out that the asymmetry of calculated $E_{2_1^+}$ values originates essentially from the difference in the adopted single-particle energies, in particular, two lowest orbits $2d_{5/2}$ and $1g_{7/2}$. We have discerned that this asymmetry is dominated by the single-particle energy term of the shell model Hamiltonian. The evolution of single-particle splitting between the $2d_{5/2}$ and $1g_{7/2}$ orbits for $N = 82$ isotones is related to the neutron-proton interactions between valence protons and neutrons in the 50–82 major shell, as suggested in Ref. [4].

ACKNOWLEDGMENTS

We are grateful for the computational resources provided by Prof. Lei from Southwest University of Science and Technology. We thank the National Natural Science Foundation of China (Grants No. 12375114, No. 11975151, No. 11961141003, and No. 11875188), the Joint Research Program with the HIRFL-CSR mass measurement in the Institute of Modern Physics, CAS, and the MOE Key Lab for Particle Physics, Astrophysics and Cosmology, for financial support.

[1] E. Wigner, Phys. Rev. **51**, 106 (1937).
[2] R. Wirowski, J. Yan, P. V. Brentano *et al.*, J. Phys. G **14**, L195 (1988).
[3] J. Yan, R. Wirowski, P. vonBrentano, A. Dewald, and A. Gelberg, Phys. Rev. C **42**, 743 (1990).
[4] R. F. Casten, J. Yan, and R. Wirowski, Nucl. Phys. A **514**, 252 (1990).
[5] M. Schimmer, R. Wirowski, P. V. Brentano *et al.*, Nucl. Phys. A **569**, 458 (1994).
[6] A. F. Lisetskiy, B. A. Brown, M. Horoi, and H. Grawe, Phys. Rev. C **70**, 044314(R) (2004).
[7] D. C. Radford, C. Baktash, J. R. Beene *et al.*, Nucl. Phys. A **746**, 83 (2004).
[8] D. C. Radford, C. Baktash, C. J. Barton *et al.*, Nucl. Phys. A **752**, 264 (2005).
[9] A. Banu, J. Gerl, C. Fahlander *et al.*, Phys. Rev. C **72**, 061305(R) (2005).
[10] J. Cederkäll, A. Ekström, C. Fahlander *et al.*, Phys. Rev. Lett. **98**, 172501 (2007).
[11] C. Vaman, C. Andreoiu, D. Bazin *et al.*, Phys. Rev. Lett. **99**, 162501 (2007).

[12] A. Ekström, J. Cederkäll, C. Fahlander *et al.*, Phys. Rev. Lett. **101**, 012502 (2008).
[13] P. Doornenbal, P. Reiter, H. Grawe *et al.*, Phys. Rev. C **78**, 031303(R) (2008).
[14] R. Kumar, P. Doornenbal, A. Jhingan *et al.*, Phys. Rev. C **81**, 024306 (2010).
[15] I. G. Darby, R. K. Grzywacz, J. C. Batchelder *et al.*, Phys. Rev. Lett. **105**, 162502 (2010).
[16] A. Jungclaus, J. Walker, J. Leske *et al.*, Phys. Lett. B **695**, 110 (2011).
[17] Y. M. Zhao, S. Yamaji, N. Yoshinaga, and A. Arima, Phys. Rev. C **62**, 014315 (2000).
[18] N. Yoshinaga and K. Higashiyama, Phys. Rev. C **69**, 054309 (2004).
[19] L. Y. Jia, H. Zhang, and Y. M. Zhao, Phys. Rev. C **75**, 034307 (2007).
[20] K. Higashiyama and N. Yoshinaga, Phys. Rev. C **83**, 034321 (2011).
[21] H. Jiang, Y. Lei, G. J. Fu, Y. M. Zhao, and A. Arima, Phys. Rev. C **86**, 054304 (2012).
[22] H. Jiang, Y. Lei, C. Qi, R. Liotta, R. Wyss, and Y. M. Zhao, Phys. Rev. C **89**, 014320 (2014).
[23] Y. Y. Cheng, C. Qi, Y. M. Zhao, and A. Arima, Phys. Rev. C **94**, 024321 (2016).
[24] M. Bao, H. Jiang, Y. M. Zhao, and A. Arima, Phys. Rev. C **101**, 014316 (2020).
[25] H. Jiang, Y. J. Zhou, Y. Lei *et al.*, Chin. Phys. C **45**, 094103 (2021).
[26] B. A. Brown, N. J. Stone, J. R. Stone, I. S. Towner, and M. Hjorth-Jensen, Phys. Rev. C **71**, 044317 (2005).
[27] S. Sarkar and M. S. Sarkar, Phys. Rev. C **64**, 014312 (2001).
[28] A. Astier, M. G. Porquet, C. Theisen *et al.*, Phys. Rev. C **85**, 054316 (2012).
[29] A. Covello, F. Andreozzi, L. Coraggio *et al.*, Prog. Part. Nucl. Phys. **38**, 165 (1997).
[30] A. Holt, T. Engeland, E. Osnes *et al.*, Nucl. Phys. A **618**, 107 (1997).
[31] L. Coraggio, A. Covello, A. Gargano, N. Itaco, and T. T. S. Kuo, Phys. Rev. C **80**, 044320 (2009).
[32] A. Ansari and P. Ring, Phys. Lett. B **649**, 128 (2007).
[33] A. Ansari, Phys. Rev. C **95**, 054309 (2017).
[34] Y. Y. Cheng, Y. M. Zhao, and A. Arima, Phys. Rev. C **94**, 024307 (2016).
[35] E. Teruya, N. Yoshinaga, K. Higashiyama, and A. Odahara, Phys. Rev. C **92**, 034320 (2015).
[36] E. E. Peters, P. Van Isacker, A. Chakraborty, B. P. Crider, A. Kumar, S. H. Liu, M. T. McEllistrem, C. V. Mehl, F. M. Prados-Estevez, T. J. Ross, J. L. Wood, and S. W. Yates, Phys. Rev. C **98**, 034302 (2018).
[37] E. E. Peters, A. E. Stuchbery, A. Chakraborty, B. P. Crider, S. F. Ashley, A. Kumar, M. T. McEllistrem, F. M. Prados-Estevez, and S. W. Yates, Phys. Rev. C **99**, 064321 (2019).
[38] A. E. Stuchbery and J. L. Wood, Physics **4**, 697 (2022).
[39] C. Ma, Y. Lu, Y. Lei, and Y. M. Zhao, Phys. Rev. C **107**, 034316 (2023).
[40] I. Talmi, Nucl. Phys. A **172**, 1 (1971).
[41] K. Allart, E. Boeker, G. Bonsignori *et al.*, Phys. Rep. **169**, 209 (1988).
[42] J. N. Ginocchio, Ann. Phys. (NY) **126**, 234 (1980).
[43] C. L. Wu, Da Hsuan Feng, X. G. Chen, J. Q. Chen, and M. W. Guidry, Phys. Rev. C **36**, 1157 (1987).
[44] F. Iachello and I. Talmi, Rev. Mod. Phys. **59**, 339 (1987).
[45] J. Q. Chen, Nucl. Phys. A **626**, 686 (1997).
[46] Y. M. Zhao, N. Yoshinaga, S. Yamaji, J. Q. Chen, and A. Arima, Phys. Rev. C **62**, 014304 (2000).
[47] G. J. Fu, Y. Lei, Y. M. Zhao, S. Pittel, and A. Arima, Phys. Rev. C **87**, 044310 (2013).
[48] Y. Y. Cheng, Y. M. Zhao, and A. Arima, Phys. Rev. C **97**, 024303 (2018).
[49] B. C. He, Lei Li, Y. A. Luo, Y. Zhang, F. Pan, and J. P. Draayer, Phys. Rev. C **102**, 024304 (2020).
[50] Y. Lei, Y. Lu, and Y. M. Zhao, Chin. Phys. C **45**, 054103 (2021).
[51] C. Ma, X. Yin, and Y. M. Zhao, Phys. Rev. C **108**, 034308 (2023).
[52] Y. M. Zhao and A. Arima, Phys. Rep. **545**, 1 (2014).
[53] http://www.nndc.bnl.gov/ensdf/.
[54] W. J. Baldridge, Phys. Rev. C **18**, 530 (1978).
[55] Chong Qi and Z. X. Xu, Phys. Rev. C **86**, 044323 (2012).
[56] X. Yin, C. Ma, and Y. M. Zhao, Phys. Rev. C **109**, 024322 (2024).
[57] https://www-nds.iaea.org/nuclearmoments/.
[58] B. Buck and S. M. Perez, Phys. Rev. Lett. **50**, 1975 (1983); S. M. Perez, Phys. Rev. C **36**, 1202 (1987); B. Buck, A. C. Merchant, and S. M. Perez, *ibid.* **63**, 037301 (2001); S. M. Perez, W. A. Richter, B. A. Brown, and M. Horoi, *ibid.* **77**, 064311 (2008); **82**, 064305 (2010).
[59] I. Talmi, *Simple Models of Complex Nuclei* (Harwood Academic, Chur, Switzerland, 1993).
[60] K. H. Speidel, O. Kenn, and F. Nowackiz, Prog. Part. Nucl. Phys. **49**, 91 (2002).
[61] Y. Nagai, J. Styczen, M. Piiparinen, P. Kleinheinz, D. Bazzacco, P. v. Brentano, K. O. Zell, and J. Blomqvist, Phys. Rev. Lett. **47**, 1259 (1981).
[62] A. Odahara, Y. Gono, S. Mitarai *et al.*, Nucl. Phys. A **620**, 363 (1997).
[63] W. H. Long, T. Nakatsukasa, H. Sagawa *et al.*, Phys. Lett. B **680**, 428 (2009).
[64] J. Dobaczewski, I. Hamamoto, W. Nazarewicz, and J. A. Sheikh, Phys. Rev. Lett. **72**, 981 (1994).
[65] I. Dillmann, K. L. Kratz, A. Wöhr *et al.*, Phys. Rev. Lett. **91**, 162503 (2003).
[66] J. Taprogge, A. Jungclaus, H. Grawe *et al.*, Phys. Rev. Lett. **112**, 132501 (2014).
[67] L. Eßer, R. V. Jolos, and P. V. Brentano, Nucl. Phys. A **650**, 157 (1999).
[68] T. Matsuzawa, H. Nakada, H. Ogawa, and G. Momoki, Phys. Rev. C **62**, 054304 (2000).